Strong Modulation of Absorption and Third-Harmonic Generation in Resonant Metasurfaces based on VO_2

Margherita Marni and Domenico de Ceglia
Department of Information Engineering, University of Padova, Italy

Keywords: Metasurfaces, Nonlinear Optics, Harmonic Generation, Nanoantennas, Tunable Devices, Nanophotonics, Phase-change Materials.

Abstract: Control of linear and nonlinear optical signals is of key importance in a variety of applications, including signal processing, optical computing and energy harvesting, to name just a few. Optical modulation and switching, and more generally tunability in photonic devices, are usually achieved in the visible and near-infrared range by carrier injection, chemical or mechanical activation, or by deploying materials with large electro-optic or optical nonlinear coefficients. However, these mechanisms are inherently weak and therefore require intense control signals in order to produce significant modulation effects. Here we adopt a nanophotonic solution in which a resonant film of a volatile phase-change material, vanadium dioxide, is inserted between an array of antennas and a metallic backplane. Our design takes advantage of (i) the large refractive-index change of VO_2 at its insulator-to-metal transition and (ii) the field enhancements available when the Fabry-Pérot resonance of the film and the plasmonic resonance of the antennas are exited. In response to the VO_2 phase transition, not only does our metasurface provide a strong and broadband modulation of linear absorption and reflection but it also shows a drastic variation of third-harmonic generation, with a conversion-efficiency contrast higher than three orders of magnitude.

1 INTRODUCTION

Metasurfaces and their constituent metamolecules, i.e., nanoantennas, are able to control light-matter interactions at the nanoscale (Yu et al., 2011). Amplitude, phase and polarization of light can be manipulated at will by properly designing these nanostructures. Dynamic control of metasurfaces' functionalities holds the promise to unlock a wide variety of new opportunities for highly compact photonic devices, capable of modulating, beaming and switching light. Here we discuss the modulation properties of a plasmonic metasurface that incorporates vanadium dioxide. This phase-change material is particularly attracting for the design of low-power tunable devices because it exhibits an abrupt and reversible change of its complex refractive index at the relatively low temperature of 68 °C. So far, a number of designs of VO_2-based metasurfaces has been investigated. The design strategies to achieve tunability at optical frequencies are based on the use of either planar structures (Kats et al., 2013; Kats et al., 2012; Kocer et al., 2015), in which one of the films is made of VO_2, or patterned nanostructures (i.e., metasurfaces), typically designed with hybrid VO_2-metal resonators – see, for example (Zhu et al., 2017). The metasurface proposed here is configured as a perfect absorber, known as Salisbury screen at microwave frequency, with a thin film of VO_2 sandwiched between a two-dimensional array of plasmonic antennas and a metallic substrate that acts as a mirror. In this configuration, the metasurface provides two types of resonances: Fabry-Pérot (FP) resonances with field localization in the VO_2 film; antenna resonances (AR), with the field highly confined around the plasmonic antennas. Thanks to the coupling of these two resonances, high absorption is achieved in a broad band of near-infrared wavelengths, when VO_2 is in its insulating phase. On the other hand, when VO_2 switches to the metallic phase, for temperatures larger than 68 °C , the metasurface tends to reflect light more efficiently, and therefore absorption drops significantly.

In addition, we have investigated the modulation of third-harmonic generation (THG) due to the cubic nonlinearity of VO_2. If the pump signal at the fundamental wavelength is tuned at the AR of the metasurface, a large contrast of third-harmonic

Marni, M. and de Ceglia, D.
Strong Modulation of Absorption and Third-Harmonic Generation in Resonant Metasurfaces based on VO2.
DOI: 10.5220/0010340000400045
In *Proceedings of the 9th International Conference on Photonics, Optics and Laser Technology (PHOTOPTICS 2021)*, pages 40-45
ISBN: 978-989-758-492-3

conversion efficiency is obtained in response to the VO_2 insulator-to-metal transition.

2 DESCRIPTION OF THE METASURFACE

The tunable absorber metasurface, reported in Figure 1, is composed of a substrate made of gold, a thin-film layer of VO_2 and an array of gold antennas with a cross shape. The design has been made so that the structure is insensitive to the input polarization, with each antenna resonating near $\lambda = 1.55$ µm. The antenna has a square cross-section with size 30x30 nm and the length of the cross arms is 145 nm. The antenna length has been designed by maximizing, at 1.55 µm, the average field-enhancement calculated in the rods volume. The period of the unit cell is 300 nm in both the x and y directions, so that the metasurface shows only zero-th order reflection at normal incidence, at both the pump and the third-harmonic (TH) wavelengths.

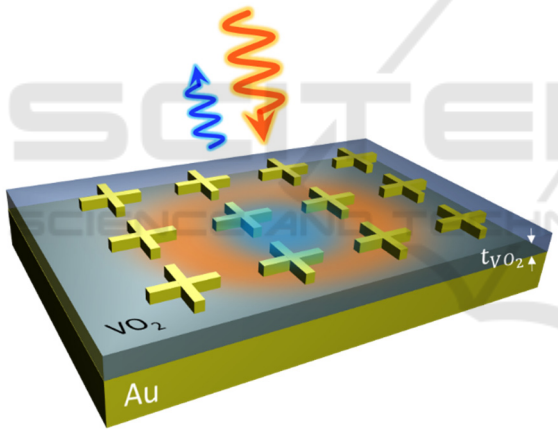

Figure 1: Schematics of the tunable metasurface under investigation. The structure is illuminated at normal incidence with a near-infrared source (red arrow). The TH signal is radiated back towards the source (blue arrow).

The simulations have been performed using COMSOL, both in the linear and nonlinear regime. Gold has been modelled with the Lorentz-Drude dispersion of (Rakić et al., 1998). For VO_2 in the insulator phase ($T < 68$ °C) and metallic phase ($T > 68$ °C), we have used the datasets made available in (Wan et al., 2019). The metasurface is illuminated with a plane wave at normal incidence, linearly-polarized along the y-direction. Linear and nonlinear spectra are calculated by using the layer thickness of VO_2, t_{VO_2}, as a free parameter that varies between 40 nm and 140 nm. In our structure, the VO_2 film acts as spacer between the antenna array and the backplane mirror, as in the Salisbury screen absorber configuration.

3 RESULTS AND DISCUSSION

3.1 Linear Response and Modulation of Absorption

The metasurface supports two types of resonances, namely, FP resonances and AR. The AR has been designed at 1.55 µm in absence of the VO_2 film and the gold backplane, and assuming a glass substrate (index 1.5). It is reasonable to expect an absorption peak near this wavelength, with strong field localization around the antennas. In addition, since there is a gold slab under the VO_2 layer, according to the *image theorem*, we can expect that our structure shows absorption peaks when the FP resonances of the film are excited, specifically when $\lambda_{FP} = 4n_{VO_2}t_{VO_2}/m$, where $m = 1,2, \ldots$ is the FP resonance order and n_{VO_2} is the VO_2 refractive index. At wavelengths near the AR and FP resonances, the metasurface behaves as a strong absorber. In Figure 2, we show the absorption spectrum in the linear regime for a VO_2 thickness equal to 80 nm.

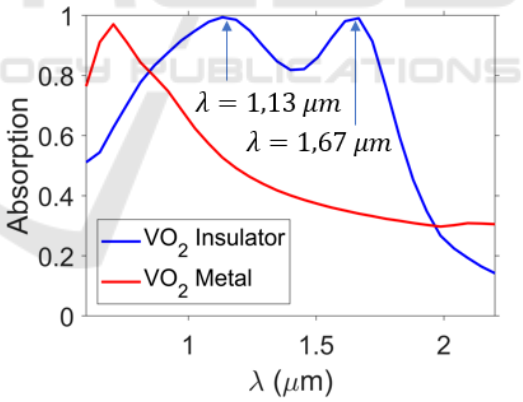

Figure 2: Calculated absorption spectrum as function of wavelength in insulator (blue line) and metal (red line) state of VO_2 when the VO_2 thickness is $80nm$.

One can note the broadband enhanced absorption effect associated with the excitation of the FP resonance and the AR. Furthermore, there is a strong difference between the spectra in the insulator and metal states of VO_2. In particular, in a broadband region, from 1 to 2 µm, the structure switches from a high absorption state, with maximum peaks close to 100%, to a low absorption state, with an average

absorption of approximately 40% in the same wavelength range. The interesting and counterintuitive aspect to observe is that the structure is very absorptive when the VO_2 is in the insulator phase, while it becomes a more efficient reflector when VO_2 switches to the metallic state.

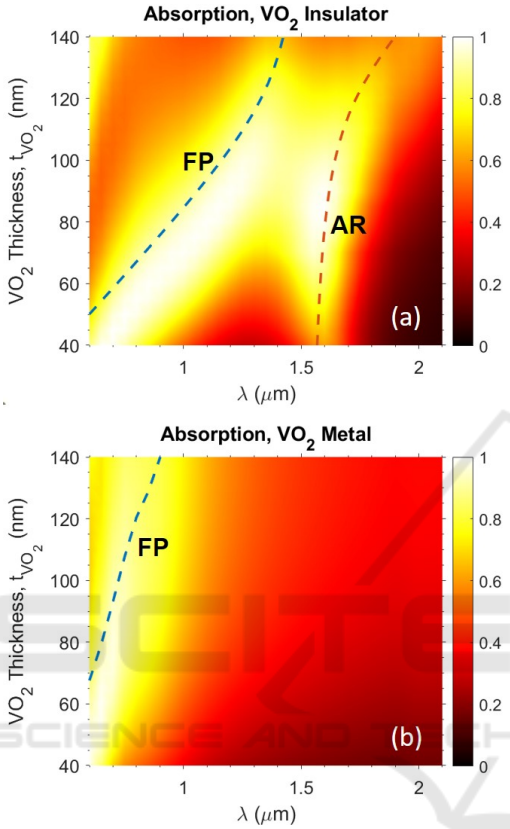

Figure 3: Absorption color map of the tunable absorber metasurface as a function of wavelength and VO_2 thickness. In (a) VO_2 is in its insulator state, in (b) VO_2 is in its metal state. In (a) the dashed lines follow the FP and AR resonances according to model in Eq. (1).

For VO_2 is in its insulator state, there are two absorption peaks, at $\lambda_{FP} = 1.13$ μm and at $\lambda_{AR} = 1.67$ μm, corresponding to the FP resonance and to the AR, respectively. It is interesting to notice that the AR appears at a longer wavelength with respect to the designed wavelength of 1.55 μm. In fact, the system is made by two coupled resonators (FP and AR), and the two resonances tend to split and repel each other when coupling is stronger, leading to the typical anticrossing effect of coupled oscillators. In order to highlight this behavior, we have calculated the absorption spectra for different values of VO_2 thickness. The results of this analysis are presented in Figure 3. When VO_2 is in the insulator state, the metasurface response can be modelled as a two coupled oscillator system, with resonance frequencies given by (Novotny, 2010):

$$\omega_{FP,AR} = \left[\frac{1}{2}\left(\omega_1^2 + \omega_2^2 \pm \sqrt{(\omega_1^2 - \omega_2^2)^2 + 4\Gamma^2\omega_1\omega_2}\right)\right]^{\frac{1}{2}} \quad (1)$$

where ω_1 and ω_2 are the FP and AR resonance frequencies in absence of mutual coupling, respectively, whereas Γ is the anticrossing frequency splitting. Here $\omega_1 = 2\pi c/\lambda_{FP}$ is the frequency of the first-order FP resonance and $\omega_2 = 2\pi c/1.55\mu m$ is the frequency of the uncoupled AR ($\Gamma = 0$). A good agreement with the numerically-calculated absorption peaks is obtained when the mutual coupling is $\Gamma \cong 0.26\,\omega_2$, as depicted in Figure 3(a), in which the dashed curves are retrieved by using Eq. (1). The anticrossing due to coupling produced a broadband absorption for wavelength from 1 to 2 μm and for a broad range of t_{VO_2} values. The AR weakly depends on t_{VO2}, and it is strongly blue-shifted when VO_2 undergoes the phase transition. The AR is completely quenched when the VO_2 film becomes metallic – see Figure 3(b).

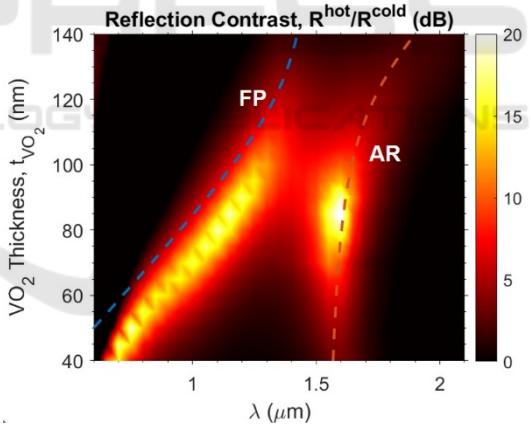

Figure 4: Reflection contrast R_{hot}/R_{cold}, on a dB color scale, for varying λ and t_{VO_2}. The dashed lines follow the FP and AR resonances according to model in Eq. (1).

A better idea of the tunability performances is provided by the modulation depth of reflectance, which is a metrics that can be retrieved experimentally. When VO_2 changes phase from insulator to metallic, the metasurface switches from a virtually perfect absorber [see Figure 2 and Figure 3(a)] to a good mirror [see Figure 3(b)]. The reflectance contrast, defined as R_{hot}/R_{cold}, where $R_{hot/cold}$ is the reflectance for VO_2 in the

insulator/metal state, is mapped in Figure 4 for varying wavelength and VO_2 film thickness. Thanks to the anticrossing of the AR and FP resonance an average ~15 dB contrast is obtained in a large bandwidth in the near infrared, with a peak of 20 dB at λ~1.6 μm with a thickness of VO_2 of 85 nm.

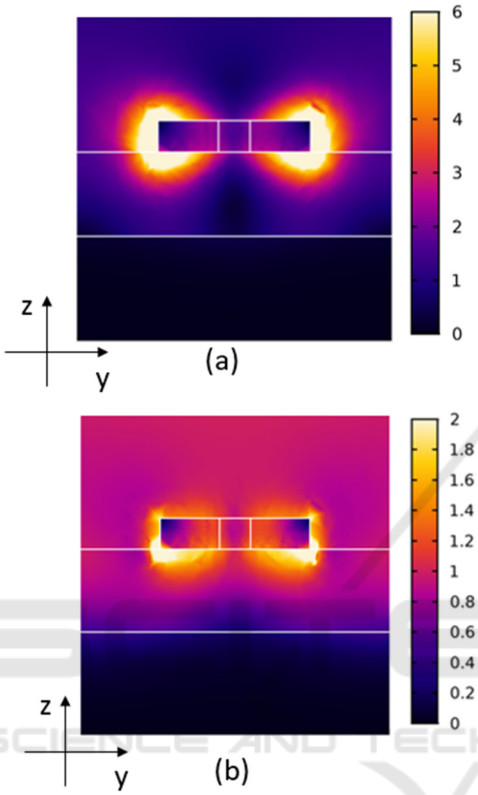

Figure 5: Field enhancement spatial calculated as the ratio between local electric field and incident one E_0, when VO_2 is in insulator state with a VO_2 film thickness equal to 80nm. (a) FE calculated at the AR wavelength. (b) same as (a) at the FP resonance wavelength.

Another important aspect of the problem is the behavior of the field enhancement (FE), calculated as the ratio between the amplitude of the local electric field and the amplitude of the incident electric field. Figure 4 compares the FE spatial distribution when the structure is under FP and AR resonance conditions. It is clear that the FE at the AR wavelength is higher than that calculated at the FP resonance. Figure 5(a) indicates that the localization and the electric-field mainly concerns the area around the antenna. On the other hand, Figure 5(b) shows that the FE is distributed throughout the volume of the VO_2 when the FP is excited. When the VO_2 passes in its metal state, the FE decreases by ~90% for the AR and by ~70% for the FP resonance.

3.2 Nonlinear Response and Modulation of Third Harmonic Generation

We now focus on the nonlinear response of the metasurface that originates from the cubic nonlinearity of VO_2. We assume an isotropic $\boldsymbol{\chi^{(3)}}$ tensor so that the induced nonlinear polarization at the TH wavelength is:

$$P_i(3\omega) = \epsilon_0 \chi^{(3)} \left[E_i^2(\omega) + E_j^2(\omega) + E_k^2(\omega)\right] E_i(\omega), \quad (2)$$

where (i, j, k) are the Cartesian coordinates, ϵ_0 the vacuum permittivity and $\chi^{(3)}$ the third-order nonlinear susceptibility of VO_2. Here we assume that $\chi^{(3)} = 10^{-19}\mathrm{m}^2/\mathrm{V}^2$ when VO_2 is in the insulator state and $\chi^{(3)} = 3.16 \times 10^{-19}\mathrm{m}^2/\mathrm{V}^2$ when VO_2 is in the metal state. The increase of $\chi^{(3)}$ that accompanies the insulator-to-metal transition has been experimentally observed in (Petrov, Yakovlev, & Squier, 2002), where third-harmonic generation from a VO_2 film measured as a function of pump irradiance and temperature. In our nonlinear simulations, the structure is pumped at normal incidence with a *y*-

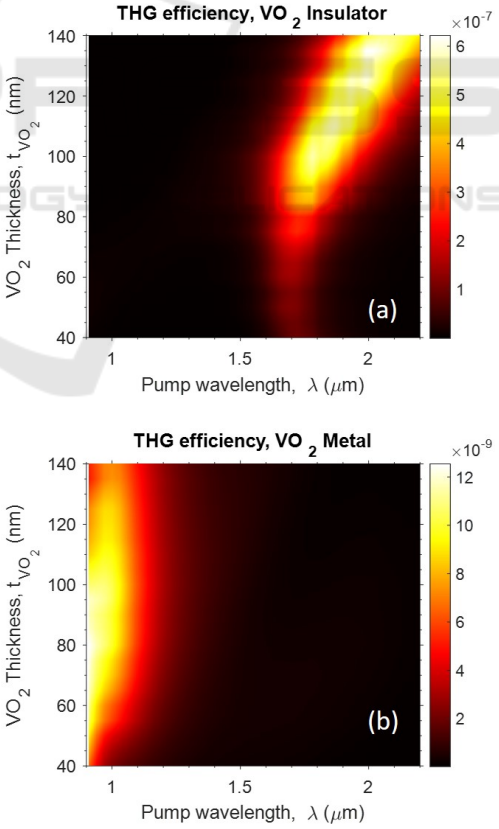

Figure 6: Color map of THG conversion efficiency as a function of pump wavelength and VO_2 thickness. (a) VO_2 is in insulator state, and (b) VO_2 is in metal state.

polarized plane wave with intensity I_0=1 GW/cm^2 and wavelength in the near-infrared, in the wavelength range where the FP and AR resonances occur. The conversion efficiency of TH generation is calculated as η_THG=P^3ω/P^ω, where P^3ω is the power of the reflected TH signal and P^ω is the incident power. In Figure 6, η_THG is mapped as a function of pump wavelength and VO2 film thickness.

With VO_2 in the insulator phase, a maximum peak of THG is observed when the pump wavelength is tuned at the AR, while no feature is associated with the FP resonance [Figure 6(a)]. Even though the $\chi^{(3)}$ increases when VO_2 switches in the metallic state, THG efficiency drops significantly near the AR wavelength and only a shallow peak appears near the FP resonance [Figure 6(b)]. These results are in agreement with the Fermi's golden rule, which predicts that the THG conversion efficiency scales as (Vincenti et al., 2014):

$$\eta_{THG} \propto \left[\chi^{(3)}\right]^2 \mathrm{FE}^6. \quad (3)$$

In response to the VO_2 transition, on one hand $\chi^{(3)}$ increases by a factor ~3, on the other hand the FE drops by 90% on the AR resonance and 70% on the FP. As a result of this FE drop, the conversion efficiency is significantly inhibited in the VO_2 metallic state. A better picture of this effect can be observed in Figure 7, where cross sections of the color maps of Figure 6 are plotted for $t_{VO_2} = 80$ nm. When the pump is tuned on the AR wavelength, the drop of reflected THG is of about three orders of magnitude (30 dB), due to the high sensitivity of THG to the FE.

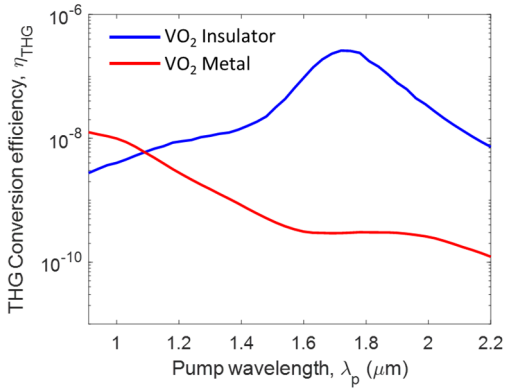

Figure 7: Color map of THG conversion efficiency as a function of pump wavelength and VO_2 thickness. (a) VO_2 is in insulator state, and (b) VO_2 is in metal state.

4 CONCLUSIONS

We have studied a tunable metasurface that exploits the insulator-to-metal transition of VO_2. The structure has been designed as a tunable absorber/mirror in the Salisbury configuration, with the VO_2 film acting as a tunable spacer between a metallic backplane and an array of metallic antennas. Our results indicate that a deep modulation of linear spectra – absorption and reflection – are obtained if the structure is judiciously designed so that Fabry-Pérot and antenna resonances are mutually coupled. A reflectance contrast of ~15 dB is found in a broad bandwidth in the near-infrared range. An even stronger modulation effect is predicted for the reflected third-harmonic generation. The conversion efficiency of this nonlinear process drops by ~30 dB when the metasurface is pumped near the antenna resonance.

ACKNOWLEDGEMENTS

The authors acknowledge the project "Internet of Things: Sviluppi Metodologici, Tecnologici E Applicativi", cofunded (2018–2022) by the Italian Ministry of Education, Universities and Research (MIUR) under the aegis of the "Fondo per il finanziamento dei dipartimenti universitari di eccellenza" initiative (Law 232/2016). The work was partially sponsored by the RDECOM-Atlantic, US Army Research Office, and Office of Naval Research Global.

REFERENCES

Kats, M. A., Blanchard, R., Genevet, P., & Capasso, F. (2013). Nanometre optical coatings based on strong interference effects in highly absorbing media. *Nat. Mater.*, *12*(1), 20-24.

Kats, M. A., Sharma, D., Lin, J., Genevet, P., Blanchard, R. Yang, Z., Qazilbash, M.M., Basov, D.N., Ramanathan, S., & Capasso, F. (2012). Ultra-thin perfect absorber employing a tunable phase change material. *Appl. Phys. Lett.*, *101*(22), 221101.

Kocer, H., Butun, S., Palacios, E., Liu, Z., Tongay, S., Fu, D., Wang, K., Wu, J., & Aydin, K. (2015). Intensity tunable infrared broadband absorbers based on VO 2 phase transition using planar layered thin films. *Sci. Rep.*, *5*(1), 1-7.

Novotny, L. (2010). Strong coupling, energy splitting, and level crossings: A classical perspective. *Am. J. Phys.*, *78*(11), 1199-1202.

Petrov, G. I., Yakovlev, V. V., & Squier, J. (2002). Nonlinear optical microscopy analysis of ultrafast

phase transformation in vanadium dioxide. *Opt. Lett.*, *27*(8), 655-657.

Rakić, A. D., Djurišić, A. B., Elazar, J. M., & Majewski, M. L. (1998). Optical Properties of Metallic Films for Vertical-Cavity Optoelectronic Devices. *Appl. Optics, 37*(22), 5271-5283.

Vincenti, M. A., de Ceglia, D., Grande, M., D'Orazio, A., & Scalora, M. (2014). Third-harmonic generation in one-dimensional photonic crystal with graphene-based defect. *Phys. Rev. B, 89*(16), 165139.

Wan, C., Zhang, Z., Woolf, D., Hessel, C. M., Rensberg, J., Hensley, J. M., Xiao, Y., Shahsafi, A., Salman, J., Richter, Sun, Y., Qazilbash, M. M., Schmidt-Grund, R., Ronning, C., Ramanathan, S., & Kats, M. A. (2019). On the Optical Properties of Thin - Film Vanadium Dioxide from the Visible to the Far Infrared. *Ann. der Phys.*, *531*(10), 1900188.

Yu, N., Genevet, P., Kats, M. A., Aieta, F., Tetienne, J.-P., Capasso, F., & Gaburro, Z. (2011). Light propagation with phase discontinuities: generalized laws of reflection and refraction. *Science*, *334*(6054), 333-337.

Zhu, Z., Evans, P. G., Haglund Jr, R. F., & Valentine, J. G. (2017). Dynamically reconfigurable metadevice employing nanostructured phase-change materials. *Nano Lett.*, *17*(8), 4881-4885.